The Effect of Dynamic Surface Tension on the Oscillation of Slender Elliptical Newtonian Jets †

S. E. Bechtel[1], M. G. Forest[2], N. T. Youssef[1], H. Zhou[2]

[1] Department of Aerospace Engineering, Applied Mechanics, and Aviation, The Ohio State University, Columbus, OH 43210

[2] Department of Mathematics, University of North Carolina, Chapel Hill, NC 27599-3250

Abstract

We investigate free surface oscillating jets with elliptical cross section, focusing on behavior associated with decaying surface tension. Previous one-dimensional equations for an oscillating jet are extended to allow variable surface tension on short space and time scales relevant for surfactant mixtures. We presume the decay of surface tension as a function of surface age, and derive the resulting jet behavior. Three plausible forms of decay are studied: an exponential decay, a diffusion model derived in Brazee *et al.* (1994), and an algebraic form due to Hua and Rosen (1991). Our simulations suggest both experimental regimes, and measurable jet features in these regimes, which may be exploited in an inverse formulation to deduce the unknown rapid surface tension decay of a given surfactant mixture. In particular, we establish numerical relationships between the amplitude and the wavelength of either a sustained farfield oscillation or oscillation at a fixed downstream location and the entire history of surface tension decay. These numerical relationships are ideal for the inverse formulation, in that the complete surface tension evolution may be deduced solely from farfield or downstream jet measurements, away from the confined part of the jet where the surface tension is rapidly changing.

1 Introduction

To model and understand agricultural and industrial processes such as spraying, fiber spinning, and film blowing, it is necessary to resolve the sizable and rapid change of material properties over small time and distance scales. The surface tension of pesticide solutions in air varies

† Appeared in Journal of Applied Mechanics, 65, 1–11, 1998

with surface age, from an initial value near that of pure water (72 dyne cm^{-1}) when the surface is created to an equilibrium value as low as 20 dyne cm^{-1} at 70 ms. Significant decay in surface tension occurs in the first 2-5 ms, which coincides with the timescale of drop formation and atomization (Thomas and Potter (1975); Brazee *et al.* (1994); Reichard *et al.* (1997)). Since surface tension dominates the hydrodynamic instability leading to droplets, accurate methods for the determination of surface tension on submillisecond timescales are necessary; slow or static techniques such as the Du-Nouy ring (Lunkenheimer and Wantke (1981)) yield only the equilibrium surface tension.

Measurements of oscillating free surface jets have long been used in inverse problems to deduce surface tension (Rayleigh (1879); Bohr (1909); Hansen *et al.* (1958); Defay and Hommelen (1958); Thomas and Potter (1975); Bechtel *et al.* (1995)). An experimentalist can prepare conditions (specified in the text below) under which a fluid exiting an elliptical orifice establishes a steady jet with a chain-like free surface fixed in space: the jet cross section oscillates in the downstream direction between perpendicular ellipses (Rayleigh (1879)). This jet flow is elongational. Features of the steady free surface profile, such as the local wavelength of the oscillation, can be conveniently measured and are strongly tied to the local interfacial surface tension.

The oscillating jet technique is the only experimental tool for the measurement of dynamic surface tension both on the rapid timescales and in an elongational flow relevant to industrial and agricultural processes of spraying, fiber spinning, and film blowing. To exploit the technique, one combines measurements of the oscillating jet profile with an analytical model that governs the evolution of the jet cross section for prescribed material properties; material coefficients are then determined so that the model and experiment agree. Importantly, all previous models predict oscillating jet behavior under the assumption that surface tension and viscosity are constant in the spatial interval over which measurements are taken. These models quantify the decay of surface tension only on the resolution of a wavelength of oscillation; for typical flow rates and orifice sizes, this results in an averaging over a time interval of 1.5 to 2 ms, during which the surface tension can drop 20-30% (Brazee *et al.* (1994)).

This paper provides the model formulation necessary to resolve dynamic surface tension within a wavelength and on submillisecond timescales. We assume a surface tension decay as a function of surface age is given; three different surface tension decay forms are studied. To implement the inverse formulation of the model in conjunction with oscillating jet experiments, one must: (i) identify physical regimes and corresponding models specific to those experimental regimes, and (ii) establish features of the models which can be reliably measured and which can be inverted to characterize the surface tension form and decay parameters. To prepare for the inverse formulation, this paper identifies the regimes, thereby dictating how the experiment

is to be designed, and further provides numerically–generated relationships between the decay parameters and the free surface profile of the oscillating jet. In particular we find that the complete evolution of surface tension, from its initial value at the nozzle exit to its stabilized equilibrium value, can be deduced solely from farfield wavelength and amplitude measurements, or measurements at a fixed downstream position. Although this is accomplished specifically for the three forms of surface tension, the methodology applies for any surface tension decay form that may emerge from fundamental studies.

2 One-dimensional models for the oscillating jet

The fluid is assumed incompressible, and flows in the direction of gravity $\mathbf{g}$. We define space-fixed (Eulerian) Cartesian coordinates $\mathbf{x} = (x_1, x_2, x_3)$ with corresponding unit base vectors $\mathbf{e}_1, \mathbf{e}_2, \mathbf{e}_3$ such that the $\mathbf{e}_3$ direction coincides with the centerline of the jet. We assume the jet cross section is elliptical for several oscillations; the free surface of the jet is therefore posited in the form

$$\frac{x_1^2}{\Phi_1^2(x_3,t)} + \frac{x_2^2}{\Phi_2^2(x_3,t)} - 1 = 0, \tag{1}$$

where $\Phi_1(x_3,t)$ and $\Phi_2(x_3,t)$ are the principal semi-axes, coincident with the x_1, x_2 axes. (An estimate for inviscid fluids of the inherent error in this assumption is given in Bechtel *et al.* (1995).)

Recall that the oscillating jet experiment we are modeling here is steady in the Eulerian sense. In the steady case Φ_1 and Φ_2 in (1) are functions only of x_3. However, in equations (1) through (15) we retain time dependence in the problem formulation, in anticipation of future stability studies; after (15) we suppress time dependence to model the steady experiment at hand.

Also, this paper is part of an overall effort in material characterization which requires the ability to model non-Newtonian viscosity. Hence in this derivation we allow for variable viscosity,

$$\hat{\mathbf{T}} = 2\eta(\mathbf{x},t)\mathbf{D}, \tag{2}$$

even though in this paper we only present solutions in the Newtonian special case. In (2) $\hat{\mathbf{T}}$ is the determinate part of the Cauchy stress tensor $\hat{\mathbf{T}} - p\mathbf{I}$, $\mathbf{D}$ is the symmetric part of the velocity gradient, and $\eta(\mathbf{x},t)$ is the viscosity.

On the free surface (1) the kinematic boundary condition is

$$(\frac{\partial}{\partial t} + \mathbf{v}\cdot\nabla)(\frac{x_1^2}{\Phi_1^2(x_3,t)} + \frac{x_2^2}{\Phi_2^2(x_3,t)} - 1) = 0, \tag{3}$$

and the kinetic boundary condition modeling the surface tension (Edwards *et al.* (1991); Milliken *et al.* (1993)) is

$$(\mathbf{T}_{ambient} - \hat{\mathbf{T}} + p\mathbf{I})\mathbf{n} = \sigma\kappa\mathbf{n} - \nabla_s\sigma. \tag{4}$$

In (3), $\mathbf{v}$ is the velocity and ∇ is the Eulerian gradient; in (4), $\mathbf{T}_{ambient}$ is the Cauchy stress tensor in the ambient atmosphere, $\mathbf{n}$ is the outward normal to the free surface, σ is the surface tension of the fluid/ambient interface (assumed to vary only with axial length x_3 and time t), κ is the mean curvature of the free surface, and $\nabla_s\sigma$ is the gradient operator on the free surface defined by (Stone and Leal (1990))

$$\nabla_s\sigma = (\mathbf{I} - \mathbf{n}\otimes\mathbf{n})\nabla\sigma. \tag{5}$$

We assume the ambient is passive, so that the stress of the ambient atmosphere is

$$\mathbf{T}_{ambient} = -p_a\mathbf{I}, \tag{6}$$

where p_a is a constant pressure. As speeds increase in the experiment, assumption (6) becomes inadequate, and must be replaced with an empirically derived air drag model (e.g. Kase and Matsuo (1967)).

We employ the slender-filament perturbation theory described in Bechtel *et al.* (1995). We recall those features necessary to connect models with experiments. The small parameter is the slenderness ratio ε,

$$\varepsilon = \frac{r_0}{z_0} \ll 1, \tag{7}$$

where r_0 and z_0 are typical length scales in the jet cross section and in the axial direction, specifically selected at the end of this section. The Eulerian coordinates x_1, x_2, x_3, t and transverse free surface semi-axes Φ_1 and Φ_2 are scaled using the above characteristic length scales and a characteristic time scale t_0:

$$\begin{aligned} x_1 = r_0\,x\ , \quad x_2 = r_0\,y\ , \quad x_3 = z_0\,z\ , \quad t = t_0\,\tau, \\ \Phi_1(x_3,t) = r_0\,\phi_1(z,\tau)\ , \quad \Phi_2(x_3,t) = r_0\,\phi_2(z,\tau), \end{aligned} \tag{8}$$

where x, y, z, τ and ϕ_1, ϕ_2 are dimensionless. The velocity to leading order is assumed to be of the form

$$\mathbf{v} = \frac{z_0}{t_0}\{[\varepsilon x\zeta_1(z,\tau) + O(\varepsilon^3)]\mathbf{e}_1 + [\varepsilon y\zeta_2(z,\tau) + O(\varepsilon^3)]\mathbf{e}_2 + [v(z,\tau) + O(\varepsilon^2)]\mathbf{e}_3\}, \tag{9}$$

where ζ_1, ζ_2, v are dimensionless $O(1)$ functions of axial coordinate z and time τ.

The kinematic boundary condition (3) and incompressibility constraint yield the leading order equations

$$\begin{aligned}\phi_{1,\tau} + v\,\phi_{1,z} - \phi_1\,\zeta_1 = 0,\\ \phi_{2,\tau} + v\,\phi_{2,z} - \phi_2\,\zeta_2 = 0,\\ \zeta_1 + \zeta_2 + v_{,z} = 0,\end{aligned} \tag{10}$$

where "$,z$" denotes differentiation with respect to z, and "$,\tau$" with respect to τ.

The three-dimensional vector momentum equation

$$\rho(\frac{\partial \mathbf{v}}{\partial t} + \mathbf{v}\cdot\nabla\mathbf{v}) = \nabla\cdot\hat{\mathbf{T}} - \nabla p + \rho\mathbf{g}, \tag{11}$$

is reduced to one-dimensional scalar equations by integration over the jet cross section and use of the kinetic boundary condition (4). In nondimensional form these equations are:

$$\begin{aligned}B(P - 2Z\phi_1\phi_2\zeta_1) + \frac{\phi_1\phi_2}{W}K_c - \varepsilon^2\phi_1\phi_2\frac{W_{,z}}{W^2}Y_c + \varepsilon^2 B\frac{\phi_1^3\phi_2}{4}(Z_{,z}\zeta_{1,z} + \zeta_{1,zz}Z) = \frac{\phi_1^3\phi_2}{4}(\zeta_{1,\tau}\\ +\ v\zeta_{1,z} + \zeta_1^2) + O(\varepsilon^2),\\ B(P - 2Z\phi_1\phi_2\zeta_2) + \frac{\phi_1\phi_2}{W}K_s - \varepsilon^2\phi_1\phi_2\frac{W_{,z}}{W^2}Y_s + \varepsilon^2 B\frac{\phi_1\phi_2^3}{4}(Z_{,z}\zeta_{2,z} + \zeta_{2,zz}Z) = \frac{\phi_2^3\phi_1}{4}(\zeta_{2,\tau}\\ +\ v\zeta_{2,z} + \zeta_2^2) + O(\varepsilon^2),\\ \varepsilon^2\frac{1}{W}(\phi_1\phi_{2,z}K_s + \phi_2\phi_{1,z}K_c) - \varepsilon^2\frac{W_{,z}}{W^2}\int_0^{2\pi}\frac{1}{\tilde{\triangle}}(\phi_2^2\cos^2\theta + \phi_1^2\sin^2\theta)d\theta + B\varepsilon^2(2\phi_1\phi_2 Z_{,z}v_{,z}\\ +\ 2\phi_1\phi_2 Z v_{,zz} - P) + \frac{1}{F}\phi_1\phi_2 = (v_{,\tau} + vv_{,z})\phi_1\phi_2.\end{aligned} \tag{12}$$

The dimensionless parameters and functions in (12) are

$$\begin{aligned}B = \frac{t_0^2 f_0}{\rho r_0^4}\quad,\quad \frac{1}{W}(z,\tau) = \frac{\sigma(z,\tau)\,t_0^2}{\rho r_0^3},\quad \frac{W_{,z}}{W^2}(z,\tau) = \frac{\sigma_{,z}(z,\tau)\,t_0^2}{\rho r_0^3},\\ \frac{1}{F} = \frac{g t_0^2}{z_0},\quad Z(z,\tau) = \frac{\eta(z,\tau) r_0^2}{t_0 f_0},\quad Z_{,z}(z,\tau) = \frac{\eta_{,z}(z,\tau) r_0^2}{t_0 f_0},\end{aligned} \tag{13}$$

where f_0 is a characteristic force scale, to be made explicit along with the other characteristic scales later in this section. Note that

$$B\cdot Z = \frac{\eta(z,\tau)\,t_0}{\rho\, r_0^2} = \frac{1}{R}, \tag{14}$$

where R is the Reynolds number. The nondimensional pressure resultant P and functions K_c, K_s, Y_c, Y_s, and $\tilde{\triangle}$ are defined by

$$P \;=\; \frac{1}{\pi f_0}\int\int (p - p_a)dx_1 dx_2,$$

$$
\begin{aligned}
K_c &= \frac{1}{\pi}\int_0^{2\pi} \tilde{\kappa}\cos^2\theta d\theta = -\frac{\phi_1\phi_2}{\pi}\int_0^{2\pi} \frac{\cos^2\theta}{(\phi_1^2\sin^2\theta+\phi_2^2\cos^2\theta)^{3/2}}d\theta + O(\varepsilon^2),\\
K_s &= \frac{1}{\pi}\int_0^{2\pi} \tilde{\kappa}\sin^2\theta d\theta = -\frac{\phi_1\phi_2}{\pi}\int_0^{2\pi} \frac{\sin^2\theta}{(\phi_1^2\sin^2\theta+\phi_2^2\cos^2\theta)^{3/2}}d\theta + O(\varepsilon^2),\\
Y_c &= \frac{1}{\pi}\int_0^{2\pi} \frac{(\phi_1\phi_{2,z}\sin^2\theta+\phi_2\phi_{1,z}\cos^2\theta)}{(\phi_1^2\sin^2\theta+\phi_2^2\cos^2\theta+O(\varepsilon)^2)^{1/2}}\cos^2\theta d\theta,\\
Y_s &= \frac{1}{\pi}\int_0^{2\pi} \frac{(\phi_1\phi_{2,z}\sin^2\theta+\phi_2\phi_{1,z}\cos^2\theta)}{(\phi_1^2\sin^2\theta+\phi_2^2\cos^2\theta+O(\varepsilon^2))^{1/2}}\sin^2\theta d\theta,\\
\tilde{\triangle} &= (\phi_2^2\cos^2\theta+\phi_1^2\sin^2\theta+O(\varepsilon^2))^{1/2}.
\end{aligned}
\tag{15}
$$

We now suppress the time dependence in the governing equations (10) and (12), to model the oscillating jet experiment. In the steady problem we select the characteristic radial length scale r_0 to be the geometric mean of the initial principal radii of the elliptical cross section, and the characteristic axial velocity $\frac{z_0}{t_0}$ to be the axial nozzle velocity, dictated by the experiment. This translates to dimensionless upstream conditions

$$
\phi_1(0)\phi_2(0) = 1, \quad v(0) = 1. \tag{16}
$$

The steady forms of (10) imply:

$$
\zeta_1 = \frac{v\phi_{1,z}}{\phi_1}, \quad \zeta_2 = \frac{v\phi_{2,z}}{\phi_2}, \quad v\phi_1\phi_2 = 1, \tag{17}
$$

where the constant in equation $(17)_3$ is fixed by the upstream conditions (16).

In the remaining leading order equations follow from the steady forms of (12), in which we have retained the leading order contributions within each physical effect, namely viscosity $(B\cdot Z)$, viscosity gradient $(B\cdot Z_{,z})$, surface tension (W^{-1}), surface tension gradient $(\frac{W_{,z}}{W^2}\ )$, constraint pressure $(B\cdot P)$, inertia (1) and gravity (F^{-1}). In a particular experiment some subset of these effects will be dominant, and thus survive in the leading-order, dominant-balance equations. A *regime* of jet behavior is determined by the order of the full set of nondimensional parameters (13), relative to the slenderness ratio ε, in the physical experiment being modeled. Once identified, each regime then specifies the dominant asymptotic balance in equations (12).

In order to observe an oscillating jet in an experiment, one must design the experiment so that inertia and surface tension dominate to leading order in the transverse momentum equations $(12)_{1,2}$. Viscosity must either balance surface tension and inertia (which leads to attenuation of the oscillations), or be a weak effect (so that the leading order behavior is inviscid). The constraint pressure term plays a fundamental role in our asymptotic analysis; this term must balance the right hand sides of $(12)_{1,2}$ (inertia terms) and the surface tension terms. Unless the

dimensionless parameter $B = \frac{t_0^2 f_0}{\rho r_0^4}$ is $O(1)$, we cannot deduce a consistent slender oscillating jet model. This constraint therefore *selects the characteristic force*, f_0, in terms of the radial scale (r_0), timescale (t_0), and density (ρ):

$$f_0 = \frac{\rho\, r_0^4}{t_0^2}, \tag{18}$$

or equivalently, we impose $B \equiv 1$.

From analysis of the transverse momentum equations $(12)_{1,2}$ above, we impose $B = 1$ and the experiment must be such that W^{-1} is $O(1)$, while Z is at most $O(1)$. Note that in the slenderness scaling these conditions automatically imply that inertia dominates surface tension and viscosity in the axial component of momentum $(12)_3$. Hence, a jet cross section evolves downstream either with constant axial velocity ($v_{,z} = 0$) if F^{-1} is less than $O(1)$, or with the free fall velocity ($v\, v_{,z} = \frac{1}{F}$) if F^{-1} is $O(1)$.

We now posit specific regimes of oscillating jet behavior, and investigate the effect of variable surface tension as predicted by the leading order equations.

3 Oscillating jets with non-constant surface tension

Recall there are *a priori* four independent scales $r_0,\ z_0,\ t_0$, and f_0 which characterize a given experiment. We have specified the force scale f_0 in terms of $r_0,\ t_0$ in (18) in order to insure that the regime is oscillatory, with the correct balance in transverse momentum. The remaining scales, which depend on the experimental conditions, dictate if viscosity, gravity, etc., join surface tension and inertia as leading order effects in the oscillating jet.

Regime 1: Surface tension and inertia-dominated jets

We first model a fluid jet with the density, viscosity, and initial surface tension of water ($\rho = .997$ g cm^{-3}, $\eta = 1.00 \times 10^{-2}$ g cm^{-1} s^{-1}, initial surface tension $= \sigma(0) = 72.8$ dyne cm^{-1}), whose surface tension decays with surface age due to evaporation of volatile species, migration of surfactant molecules to the surface, or contamination of the surface with dust. The jet has volume flow rate $Q = 0.342$ cm^3 s^{-1}, and initial elliptical semiaxes $\Phi_1(0) = 0.0225$ cm, $\Phi_2(0) = 0.0100$ cm. These experimental conditions yield the scales

$$r_0 = \sqrt{\Phi_1(0)\Phi_2(0)} = 0.0147 \text{ cm}, \quad z_0 = \frac{r_0}{\varepsilon} = 0.147 \text{ cm},$$
$$\frac{z_0}{t_0} = \frac{Q}{\pi r_0^2} = 506\ \frac{\text{cm}}{\text{s}} \text{ (so that } t_0 = 2.89 \times 10^{-4} \text{ s)}, \quad f_0 = \frac{\rho r_0^4}{t_0^2} = 0.549 \text{ dyne}, \tag{19}$$

where we have tentatively selected $\varepsilon = 0.1$. That is, the characteristic length of axial variation, z_0, identified as the wavelength of oscillation of the jet cross section, is anticipated to be on the order of ten times that of the transverse dimensions; subsequent computations validate this guess.

We assume that the surface age T at axial position $x_3 = 0$ is zero, i.e. the surface is created at the origin. For steady flows, surface age and axial position are related by

$$T = \int_0^{x_3} \frac{dx_3}{v(x_3)} = t_0 \int_0^z \frac{dz}{v(z)}. \tag{20}$$

This allows surface tension, given as a function of surface age, to be expressed as a function of axial position,

$$\sigma = \sigma(T) = \sigma(x_3) = \sigma(z).$$

The dimensionless parameters (13) are expressed as an $O(1)$ number times a power of the slenderness ratio ε:

$$\begin{aligned} \frac{1}{F} &= \frac{g t_0^2}{z_0} = 5.61 \times 10^{-4} = 5.61\varepsilon^4, \quad \frac{1}{W(0)} = \frac{\sigma(0) t_0^2}{\rho r_0^3} = 1.92 = 1.92\varepsilon^0, \\ Z &= \frac{\eta r_0^2}{t_0 f_0} = 0.0135 = 1.35\varepsilon^2, \qquad Z_{,z} = 0. \end{aligned} \tag{21}$$

From these calculations we see that in this specific experiment W^{-1} is $O(1)$, at least upstream near the nozzle, and Z and F^{-1} are less than $O(1)$. Recalling the earlier discussion, this jet is in an oscillatory regime, at least upstream: the experimental design will result in an oscillating jet with no attenuation due to viscosity and no axial acceleration due to gravity, to leading order. In this section we wish to model experiments in which variable surface tension continues down the jet as a leading order effect, but the surface tension gradient is not too large. Hence, the Weber number evolves down the jet subject to the restrictions

$$\varepsilon < \frac{1}{W(z)} < \varepsilon^{-1}, \qquad \mid \varepsilon^2 \frac{W_{,z}}{W^2(z)} \mid < \varepsilon. \tag{22}$$

For $\varepsilon = 0.1$ this translates into the dimensional bounds,

$$3.79 \ \frac{\text{dyne}}{\text{cm}} < \quad \sigma(x_3) \quad < \quad 379 \ \frac{\text{dyne}}{\text{cm}}, \qquad \mid \ \sigma(x_3)_{,x_3} \ \mid \ < \quad 2580 \frac{\text{dyne}}{\text{cm}^2}, \tag{23}$$

which must be monitored during the experiment; note that the above value $\sigma(0) = 72.8$ dyne cm^{-1} is comfortably inside $(23)_1$. Within the bounds (23) the steady leading order equations simplify to

$$v = 1, \quad \phi_1 \phi_2 = 1, \quad (1 + \phi_1^4)\phi_{1,zz} - 2\frac{\phi_{1,z}^2}{\phi_1} + \frac{4}{\pi W(z)} \phi_1^3 \left(\int_0^{2\pi} \frac{(\cos^2\theta - \sin^2\theta) d\theta}{(\phi_1^2 \sin^2\theta + \phi_1^{-2} \cos^2\theta)^{3/2}} \right) = 0, \tag{24}$$

which we label **Regime 1**. Equation $(24)_3$ is the difference of the steady leading order forms of equations $(12)_1$ and $(12)_2$, with ζ_1 and ζ_2 eliminated using $(17)_{1,2}$. Since in Regime 1 gravity is not leading order and hence axial velocity is constant to leading order, surface age is proportional to axial location:

$$T = \frac{t_0}{z_0} x_3 = t_0 z. \tag{25}$$

Equations (24) were analyzed in Bechtel *et al.* (1988) and Bechtel (1989) for the special case of constant surface tension (W=constant), in which $(24)_3$ describes a conservative nonlinear oscillator and surface tension provides the restoring force. The total conserved energy per length is

$$h = \frac{1}{8}(1+\phi_1^{-4})\phi_{1,z}^2 + \frac{4}{W}\{\frac{E(1-\phi_1^4)}{\pi\phi_1} - \frac{1}{2}\}, \tag{26}$$

where E is the complete elliptic integral of the second kind as defined in Abramowitz and Stegun (1964). The first term in (26) is the kinetic energy per length and the second term is potential energy per length, normalized so that it is non-negative.

When surface tension σ evolves, the energy per length h decays proportional to surface tension decay:

$$h_{,z} = -4\frac{W_{,z}}{W^2}\{\frac{E(1-\phi_1^4)}{\pi\phi_1} - \frac{1}{2}\} = \frac{4t_0^2}{\rho r_0^3}\sigma_{,z}\{\frac{E(1-\phi_1^4)}{\pi\phi_1} - \frac{1}{2}\}. \tag{27}$$

To produce quantitative predictions of jets with nonconstant surface tension, we now invoke specific constitutive equations for the decay of surface tension with surface age. We investigate three functional forms: (1) exponential decay; (2) the thin-film diffusion model derived by Brazee *et al.* (1994); and (3) the algebraic form proposed by Hua and Rosen (1991). We do not address the fundamental issue of the physics and chemistry responsible for the evolution of surface tension.

For each posited surface tension form, we solve *the direct problem*: we numerically integrate the governing differential equations (24) with the particular specified function $\sigma(z)$ to obtain the free surface profile $\phi_1(z)$. Features of the jet profiles are then plotted. Looking ahead to an *inverse problem* based on experimental data and this model, we seek relationships between features of model solution behavior which can be reliably measured in an experiment and the surface tension functions, namely its form and coefficients within the form. For each of the three posited surface tension forms, we establish invertible relationships between decay rates and the farfield amplitude and wavelength of the oscillating free surface.

Form 1: Exponentially decaying surface tension

First we assume an exponential decay of surface tension with surface age, equivalent in this regime to exponential decay of surface tension with axial position:

$$\sigma(x_3) = \sigma_E + (\sigma(0) - \sigma_E)e^{-\alpha x_3} \qquad \text{or} \qquad \frac{1}{W(z)} = c_1 + c_2 e^{-c_3 z}, \tag{28}$$

where the constant α is *the exponential decay rate parameter*. Note the relations $c_3 = z_0\alpha$, $c_2 = \frac{t_0^2}{\rho r_0^3}(\sigma(0) - \sigma_E)$, and $c_1 = \frac{t_0^2}{\rho r_0^3}\sigma_E$.

Form 2: Thin-film diffusion model of Brazee *et al.* (1994)

Our second form is adopted from Brazee *et al.* (1994):

$$\sigma(T) = \sigma(0) + (\sigma_E - \sigma(0))\{1 - \frac{2}{\pi}\sum_{n=0}^{\infty}\frac{(-1)^n e^{-\pi^2 D(n+\frac{1}{2})^2\frac{T}{a^2}}}{n+\frac{1}{2}}\}, \tag{29}$$

which follows from a thin-film diffusion model accounting for surface adsorption, where D is the diffusion coefficient and a is the apparent film thickness. Using the relation (25) between surface age T and axial location, we convert (29) to an expression for surface tension as a function of axial position x_3,

$$\sigma(x_3) = \sigma(0) + (\sigma_E - \sigma(0))\{1 - \frac{2}{\pi}\sum_{n=0}^{\infty}\frac{(-1)^n e^{-\pi^2 D(n+\frac{1}{2})^2\frac{t_0 x_3}{z_0 a^2}}}{n+\frac{1}{2}}\},$$

$$\text{or} \qquad \frac{1}{W(z)} = c_1 + c_2\frac{2}{\pi}\sum_{n=0}^{\infty}\frac{(-1)^n e^{-\pi^2(n+\frac{1}{2})^2 c_4 z}}{n+\frac{1}{2}}, \tag{30}$$

where c_1 and c_2 have the same relations to $\sigma(0)$ and σ_E as in the exponential form (28), and $c_4 = t_0 D a^{-2}$. For three different agrochemical surfactants, each in varying concentrations, Brazee *et al.* (1994) provide an estimate of Da^{-2}. For all solutions they assume an initial surface tension of 72.8 dyne cm^{-1} and measure equilibrium surface tension values at a surface age of 70 ms, ranging between 30.4 and 42.9 dyne cm^{-1}. By matching with experimental measurements they deduce values of Da^{-2} between 0.02 and 0.2 s^{-1}.

Form 3: Algebraic form proposed by Hua and Rosen

The third form for dynamic surface tension is a power law proposed by Hua and Rosen (1991) and employed by Shavit and Chigier (1995),

$$\sigma(T) = \sigma_E + \frac{\sigma(0) - \sigma_E}{1 + (\frac{T}{t^*})^n}, \tag{31}$$

where t^* and n are specified constants. This relation also predicts that surface tension σ decays smoothly from a specified initial value $\sigma(0)$ to a specified equilibrium value σ_E. Using the relation (20) between surface age T and axial location x_3, we have

$$\sigma(x_3) = \sigma_E + \frac{\sigma(0) - \sigma_E}{1 + (\frac{t_0 x_3}{z_0 t^*})^n}, \qquad \frac{1}{W(z)} = c_1 + \frac{c_2}{1 + (\frac{z}{c_5})^n}, \tag{32}$$

where $c_5 = \frac{t^*}{t_0}$.

Numerical Experiments

In all calculations we assume the initial surface tension to be that of water, $\sigma(0) = 72.8$ dyne cm^{-1}, and fix the equilibrium surface tension $\sigma_E = 31$ dyne cm^{-1}, consistent with common agrochemical surfactant solutions (Brazee *et al.* (1994)); in the dimensionless forms, $c_1 = 0.827$ and $c_2 = 1.115$. We explore variations in the decay forms and associated decay parameters. In the inverse problem for surface tension characterization, σ_E will be measured with static techniques, such as the Du Nouy ring, and the remaining rate parameters (α in Form 1, Da^{-2} in Form 2, and t^* and n in Form 3) will be inferred from an inverse formulation of the model coupled with experimental measurements of the oscillating jet profile.

In Figure 1 we plot the *nearfield free surface profiles* for all three forms of surface tension decay. Figure 1a gives the profiles for exponential surface tension decay, Form 1. We note that the most rapid exponential decay ($c_3 = 200$) was purposefully chosen so that the condition $(22)_2$ on surface tension gradient is violated in a very short range (here $0 \leq z \leq 0.0015$). Therefore, the flow with $c_3 = 200$ is strictly not in Regime 1 very near the nozzle, but instead is in what we will call in the following Regime 2; see the next section. All other jets plotted in Figure 1 satisfy conditions (22) everywhere along the jet, so that they are everywhere in Regime 1. Figure 1b depicts jet behavior under Form 2; we give the oscillating jet profiles for values of Da^{-2} ranging from 0.07 to 0.21 s^{-1}, consistent with the above values reported in Brazee *et al.* (1994). Figure 1c gives jet behavior for Form 3; the values of t^* and n we have chosen correspond to aqueous surfactant Tergitol NP-10 solutions with concentrations of 6mM, 12mM and 60mM (Shavit and Chigier (1995)). Figure 1 illustrates a complex dependence of amplitude and wavelength on the decay form and rate parameters. Observe that the wavelengths and amplitudes of the oscillating jets with decaying surface tension are consistently greater than those of the jet whose surface tension remains at the initial value; this is consistent with the behavior of a nonlinear mass/spring system with weakening spring constant.

To anticipate free surface features which one might measure in experiments, in Figure 2 we post-process from the solutions in Figure 1 the locations and values of each maximum amplitude of the oscillation. We extend in Figure 2 beyond the nearfield shown in Figure 1 into the farfield. A careful inspection of Figure 2 reveals that *the farfield amplitude of oscillation depends on the form and on the rate constants within a given form of surface tension.* This may be understood as follows: As surface tension decays to an equilibrium, so does energy. If one could infer the final (equilibrium) energy density h_{eq} from the surface tension decay alone, then the amplitude and wavelength of the farfield sustained oscillation could be deduced *a priori*, without integrating

the equations of motion. However, from (27) we see

$$h_{eq} = h(0) + \frac{4t_0^2}{\rho r_0^3}\int_0^\infty \sigma_{,z}(z)\{\frac{E(1-\phi_1^4)}{\pi\phi_1} - \frac{1}{2}\}dz, \tag{33}$$

so that the equilibrium energy (and equivalently the farfield amplitude and wavelength) depends on the entire history of the oscillation, and cannot be inferred merely from $h(0)$ and $\sigma(z)$; h_{eq} must be numerically computed. In Figure 3 we specialize to Form 1 and show the evolution of the energy density $h(z)$ for the solutions of Figures 1a, 2a. The four jets each decay to different equilibrium energy per length values, $h_{eq} = 0.308063$, 0.309314, 0.255606, 0.204821 for $c_3 = 0.3$, 2.1, 7.0, 200, respectively, even though each decays to the same equilibrium surface tension. For comparison, the energies per length for the oscillating jets with constant surface tensions 72.8 dyne cm^{-1} and 31 dyne cm^{-1} are the constants $h = 0.482$ and 0.2047, respectively.

The decay of surface tension is confined to the nearfield, with the equilibrium value being reached typically at a fraction of the first wavelength, at its slowest before completion of the second oscillation. It would be difficult to make measurements of the jet free surface in this small domain with the necessary accuracy for the inverse problem. The discovery that farfield oscillatory jet behavior varies with the form of the surface tension decay and decay rate parameter(s), albeit in a nontrivial way, indicates that this is unnecessary. One can quantitatively infer the decay of surface, which happens very near the nozzle, with measurements far downstream of the nozzle, measurements that can be made much more reliably.

Figure 4 shows the dependence of equilibrium wavelength, amplitude, and equilibrium energy on the exponential decay rate c_3 in Form 1. The relations are one-to-one except in a small range of c_3 inside of which the same wavelength occurs for two distinct values of c_3. The same behavior happens for amplitude. By inverting c_3 from amplitude *and* wavelength measurements, the multiplicity in the narrow band can be averted.

Figures 5–7 provide the analogous relationships for Form 2 and Form 3. *Figures 4–7 provide the basis for an inverse characterization of the surface tension decay forms and rate constants within those forms; experimental measurements provide the vertical axis information on amplitude and wavelength, which is then inverted using the figures to infer rate parameters.* A statistical procedure, e.g. least squares, could be implemented to find a best fit among these available surface tension decay forms.

As a practical matter, it is unnecessary to monitor that an equilibrium oscillation has been reached. Figures 8–11 show that the farfield relationships of Figures 4–7 are duplicated if we focus on fixed downstream observations, chosen here as the fourth/fifth cycles of oscillation.

Regime 2: An inviscid jet with dominant surface tension gradient

As mentioned above, the jet in Figure 1a with $c_3 = 200$ violates condition $(22)_2$ in the domain $0 \le z \le 0.0015$. In this narrow axial domain $1/W$ and B are $O(1)$, $\frac{W_{,z}}{W^2}$ is $O(\varepsilon^{-2})$ and $1/F, Z$ and $Z_{,z}$ are $O(\varepsilon^2)$, so that the appropriate steady leading order equations from (12) are

$$v_{,z} = -\varepsilon^2 \frac{W_{,z}}{W^2} \int_0^{2\pi} (\phi_2^2 \cos^2\theta + \phi_1^2 \sin^2\theta)^{1/2} d\theta, \qquad v\phi_1\phi_2 = 1,$$
$$\frac{1}{\phi_1}(\frac{1}{\phi_1^2} + \frac{1}{\phi_2^2})\phi_{1,zz} - \frac{2}{\phi_1^4}\phi_{1,z}^2 + (\frac{1}{\phi_2^2} - \frac{1}{\phi_1^2})\phi_2\phi_{1,z}v_{,z} - \phi_2^2 v_{,z}^2 + \frac{\phi_2}{\phi_1}v_{,zz}$$
$$+\frac{4}{W}(K_s - K_c) - \varepsilon^2 \frac{4W_{,z}}{W^2}(Y_s - Y_c) = 0, \tag{34}$$

rather than equations (24). To compute the profile for $c_3 = 200$, one integrates equations (34) in the domain $0 \le z < 0.0015$ (in which $\frac{\varepsilon^2 W_{,z}}{W^2(z)}$ is $O(1)$), and then integrates equations (24) for $z > 0.0015$ (in which $\frac{\varepsilon^2 W_{,z}}{W^2(z)}$ has decayed to below $O(1)$). For practical purposes, this effect is negligible.

Regime 3: Newtonian jets in the presence of gravity

In this section we demonstrate that an experiment not much different than Regime 1 above can lead to a regime in which viscosity and gravity couple with inertia and surface tension as leading order effects.

Consider a jet of the same fluid as above ($\rho = 0.997$ gm cm^{-3}, $\eta = 1.00 \times 10^{-2}$ g cm^{-1} s^{-1}, $\sigma(0) = 72.8$ dyne cm^{-1}) but with a larger aperture (semi-axes 1.5 and 0.97 cm) and greater volumetric flow rate ($Q = 240$ cm^3 s^{-1}). Retaining the slenderness ratio $\varepsilon = 0.1$, we compute the dimensionless parameters

$$\frac{1}{F} = 0.5\varepsilon^0, \quad \frac{1}{W(0)} = 1.0\varepsilon^0, \quad \frac{1}{R} = BZ = 0.152\varepsilon^0, \tag{35}$$

where R is the Reynolds number. Note that for this jet, $\frac{1}{R}$ and $\frac{1}{F}$ as well as B and $\frac{1}{W}$ are $O(1)$, and the steady leading order equations are, from (12) and $(17)_3$,

$$vv_{,z} = \frac{1}{F}, \qquad v\phi_1\phi_2 = 1,$$
$$v^2(\phi_1\phi_{1,zz} - \phi_2\phi_{2,zz}) + vv_{,z}(\phi_1\phi_{1,z} - \phi_2\phi_{2,z}) + \frac{8v}{R}(\frac{\phi_{1,z}}{\phi_1} - \frac{\phi_{2,z}}{\phi_2}) + \frac{4}{W(z)}(K_s - K_c) = 0 \tag{36}$$

With gravity as a leading order effect, surface age is no longer proportional to axial distance, as

in equation (25). Rather, combining (20) and $(36)_1$, we have

$$T(z) = t_0 \int_0^z \frac{dz}{\sqrt{\frac{2z}{F}+1}} = t_0 F(\sqrt{\frac{2z}{F}+1}-1). \tag{37}$$

With (37), any form of surface tension as a function of surface age can be converted to a function of axial distance. For instance, the Brazee *et al.* form (29) becomes

$$\sigma(x_3) = \sigma(0) + (\sigma_E - \sigma(0))\{1 - \frac{2}{\pi}\sum_{n=0}^{\infty} \frac{(-1)^n e^{-\pi^2 D(n+\frac{1}{2})^2 \frac{t_0 F(\sqrt{\frac{2z}{F}+1}-1)}{a^2}}}{n+\frac{1}{2}}\}. \tag{38}$$

Figure 12 shows the effect of gravity to delay the decay of surface tension with axial distance; the specific form is the Brazee *et al.* form (Form 2) with $Da^{-2} = 0.095$ s^{-1}. Figure 13 shows how this delay, together with the underlying axial acceleration of the jet, continually stretches, decreases the amplitude, and decreases the mean surface of the free surface oscillation. Figure 14 illustrates the damping effect of viscosity; the dotted line, with $F^{-1} = 0.5$ and $R^{-1} = 0.152$, is the predicted behavior of the experiment just described, with the decay of surface tension with surface age depicted in Figure 12.

For more viscous fluids it might prove impossible to design an experiment in Regime 1; the viscosity-induced drag in the capillary upstream of the nozzle will likely force larger nozzles and flow rates, elevating (as was seen in the above experiment) gravity and/or viscosity to leading order. As is evident from Figures 13 and 14, if either of gravity or viscosity is leading order, there is no equilibrium (sustained farfield oscillation), and hence there is no equivalent of Figures 4–7 to be employed in the inverse problem for surface tension decay. In such regimes, one can focus the model and experiments at a fixed downstream location and reproduce the functional equivalents of Figures 8–11.

4 Conclusion

Previous equations for oscillating jets are extended to allow for surface tension to vary in space and time; the new models are used to investigate the effect of decaying surface tension on oscillating jet behavior. Three different functional forms for the decay of surface tension with surface age are studied: an exponential decay form, a diffusion model by Brazee *et al.* (1994), and an empirical form developed by Hua and Rosen (1991). In all forms we select initial and equilibrium values of surface tension, and decay rates consistent with experimental values reported in Thomas and Hall (1979), Hua and Rosen (1991), Brazee *et al.* (1994) and Shavit and Chigier (1995). The model behavior established here indicates that the rate and form of surface

tension decay can be inferred from a combination of static and downstream measurements along with an inverse formulation of the model. This procedure avoids measurements of the jet profile near the nozzle where rapid surface tension decay takes place, and therefore appears to be practically attractive.

5 Acknowledgment

This work was funded in part by the National Science Foundation, under Grants CTS-9319128 and CTS-9711109, and the Air Force Office of Scientific Research, Air Force Materials Command, USAF, under Grants F49620-97-1-0001 and F49620-97-1-0003. The US Government is authorized to reproduce and distribute reprints for governmental purposes notwithstanding any copyright notation thereon. The views and conclusions contained herein are those of the authors and should not be interpreted as necessarily representing the official policies or endorsements, either expressed or implied, of the Air Force Office of Scientific Research or the US Government. SEB and MGF acknowledge valuable discussions with Robert Fox and Ross Brazee of the U.S. Department of Agriculture, Wooster, Ohio. All authors thank an anonymous referee for constructive suggestions.

References

Abramowitz, M. & Stegun, I. A. 1964. *Handbook of Mathematical functions.* Dover.

Bechtel, S. E. 1989. The oscillation of slender elliptical inviscid and Newtonian jets: Effects of surface tension, inertia, viscosity and gravity. *Journal of Applied Mechanics*, **56**, 968–974.

Bechtel, S. E., Lin, K. J. & Forest, M. G. 1988. On the behavior of viscoelastic free jets with elliptical cross-section. *Journal of Non-Newtonian Fluid Mechanics*, **27**, 87–126.

Bechtel, S. E., Cooper, J. A., Forest, M. G., Petersson, N. A., Reichard, D. L., Saleh, A. & Venkataramanan, V. 1995. A new model to determine dynamic surface tension and elongational viscosity using oscillating jet measurements. *Journal of Fluid Mechanics*, **293**, 379–403.

Bohr, N. 1909. Determination of dynamic surface tension by the method of jet vibration. *Transactions of the Royal Society, London*, **209**, 281–317.

Brazee, R. D., Bukovac, M. J., Cooper, J. A., Zhu, H., Reichard, D. L. & Fox, R. D. 1994. Surfactant diffusion and dynamic surface tension in spray solutions. *Transactions of the ASAE*, **37**, 51–58.

Defay, R. & Hommelen, J. 1958. Measurements of dynamic surface tensions of aqueos solutions by the oscillating jet method. *Journal of Colloid Science*, **13**, 553–564.

Edwards, D. A., Brenner, H. & Wasan, D. T. 1991. *Interfacial Transport Processes and Rheology*. Boston: Butterworth-Heinamann.

Hansen, R. S., Purchase, M. E., Wallace, T. C. & Woody, R. C. 1958. Extension of the vibrating jet method for surface tension measurements to jets of non-uniform velocity profile. *Journal of Physical Chemistry*, **62**, 210–214.

Hua, X. Y. & Rosen, M. J. 1991. Dynamic surface tension of Aqueous surfactant solutions. *Journal of Colloid and Interface Science*, **141**, 180–189.

Kase, S. & Matsuo, T. 1967. Studies on melt spinning. ii. Steady state and transient solutions of fundamental equations compared with experimental results. *Journal of Polymer Science*, **11**, 251–287.

Lunkenheimer, K. & Wantke, K. D. 1981. Determination of the dynamic surface tension of surfactant solutions applying the method of Lecomte du Nouy (ring tensiometer). *Coll. & Polymer Sci.*, **259**, 354–366.

Milliken, W. J., Stone, H. A. & Leal, L. G. 1993. The effect of surfactant on the transient motion of Newtonian drops. *Physics of Fluids A*, **5**, 69–79.

Rayleigh, Lord. 1879. On the capillary phenomena of jets. *Proceedings of the Royal Society, London*, **29**, 71–97.

Reichard, D. L., Cooper, J. A., Bechtel, S. E. & Fox, R. D. 1997. A system for determining dynamic surface tension using the oscillating jet technique. *Atomization and Sprays*, **7**, 219–233.

Shavit, U. & Chigier, N. 1995. The role of dynamic surface tension is air assist atmoization. *Physics of Fluids*, **7**, 24–33.

Stone, H. A. & Leal, L. G. 1990. The effect of surfactants on drop deformation and breakup. *Journal of Fluid Mechanics*, **220**, 161–186.

Thomas, W. D. E. & Hall, D. J. 1979. Dynamic surface tension of some non-ionic surfactant at the solution/air surface. *Surface Active Agents, Symposium, London: Soc. Chem. Ind,*, 107–116.

Thomas, W. D. E. & Potter, L. 1975. Solution/Air interfaces 1. An oscillating jet relative method for determining dynamic surface tension. *Journal of Colloid and Interface Science*, **50**, 397–412.

List of Figures

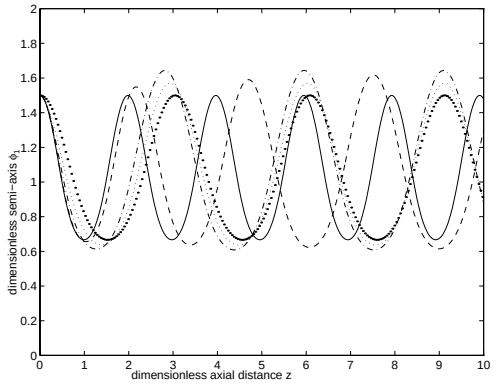

(1a)

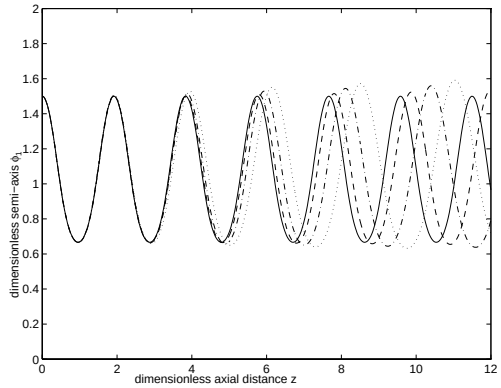

(1b)

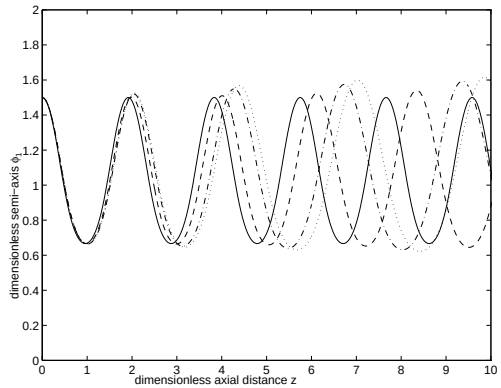

(1c)

Figure 1: Dimensionless nearfield free surface profiles $\phi_1(z)$ for inviscid jets with variable surface tension; for comparison, the profile with constant surface tension $\sigma = 72.8$ dyne cm^{-1} (——) is given. In all solutions the initial data is $\phi_1(0) = 1.5, \phi_{1,z}(0) = 0$. (Graphs can be converted to dimensional radius vs. dimensional axial distance by multiplying the z axis by 0.15 cm and the ϕ_1 axis by 0.015 cm). $\sigma(0) = 72.8$ dyne cm^{-1} and $\sigma_E = 31$ dyne cm^{-1}, so that $c_1 = 0.827$ and $c_2 = 1.115$. (a) Form 1: exponentially decaying form, with rate values $c_3 = 0.3$ (− − −), $c_3 = 2.1$ (_ . _ . _), $c_3 = 7.0$ ($\cdots$), $c_3 = 200$ (•• •); (b) Form 2: Brazee *et al.* form, with rate values $c_4 = 2.16 \times 10^{-5}$ (− − −), $c_4 = 4.12 \times 10^{-5}$ (_ . _ . _), $c_4 = 6.07 \times 10^{-5}$ ($\cdots$); (c) Form 3: Hua and Rosen form, with parameter values $c_5 = 25.9, n = 3.839$ (− − −); $c_5 = 9.667, n = 2.328$ (_ . _ . _ .); $c_5 = 4.58, n = 1.634$ ($\cdots$).

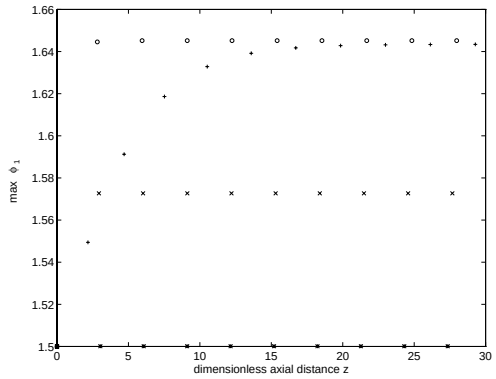

(2a)

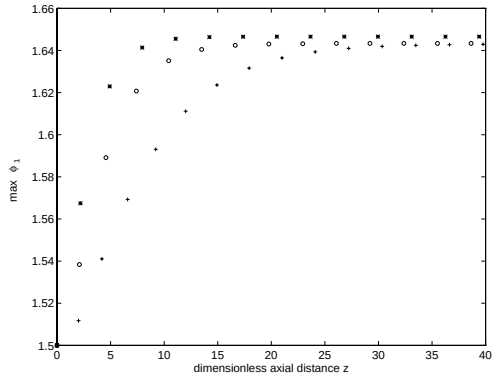

(2b)

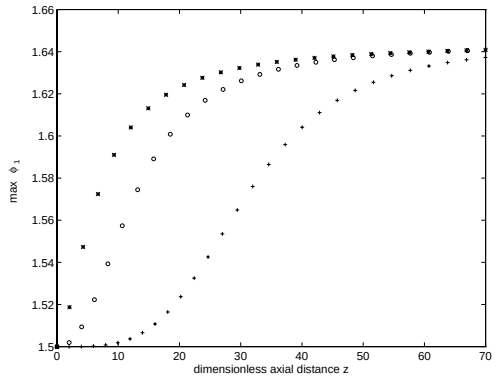

(2c)

Figure 2: Successive maximum amplitudes of each solution in Figure 1, for a much larger axial domain (nearfield and farfield). (a) Form 1: $c_3 = 0.3$ (+), $c_3 = 2.1$ ($\circ$), $c_3 = 7.0$ ($\times$), $c_3 = 200$ ($*$). (b) Form 2: $c_4 = 2.16 \times 10^{-5}$ (+); $c_4 = 4.12 \times 10^{-5}$ ($\circ$); $c_4 = 6.07 \times 10^{-5}$ ($*$). (c) Form 3: $c_5 = 26.7241, n = 3.839$ (+); $c_5 = 9.975, n = 2.328$ ($\circ$); $c_5 = 4.725, n = 1.634$ ($*$).

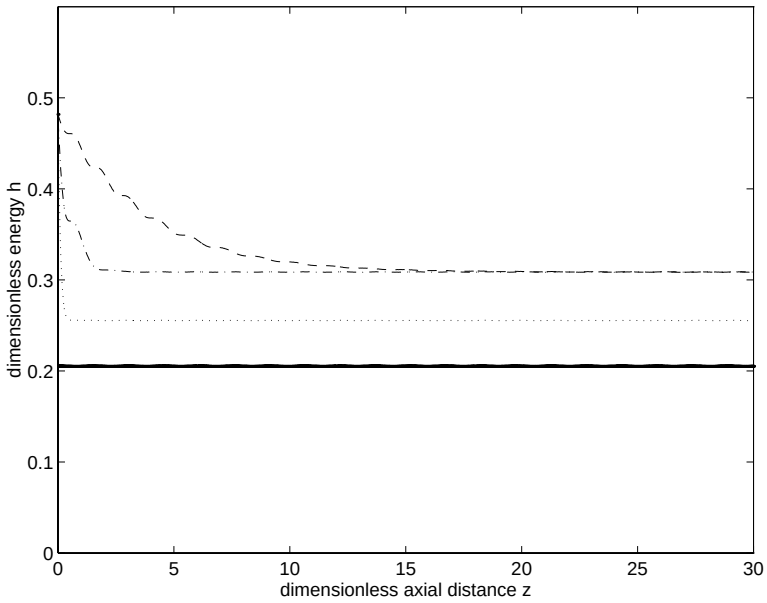

Figure 3: The decay of energy per length (26) for the oscillating jets of Figure 1a with exponentially decaying surface tension. $c_3 = 0.3$ (− − −), $c_3 = 2.1$ (_ . _ . _), $c_3 = 7.0$ ($\cdots$), $c_3 = 200$ (• • •).

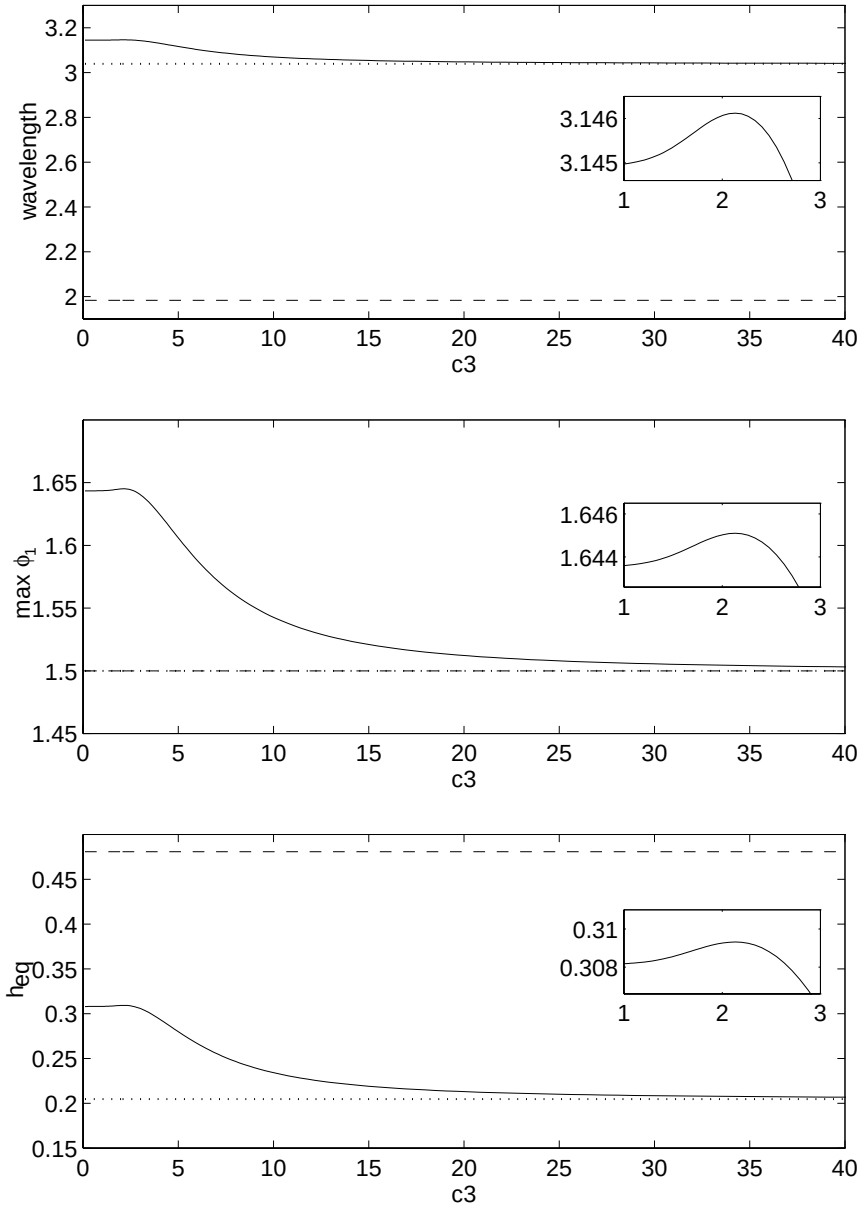

Figure 4: Dependence of the sustained farfield oscillation on c_3 of a jet with exponentially decaying surface tension. The top, middle, and bottom graphs show the dependence of farfield wavelength, amplitude, and energy, respectively, for $c_3 > 0.1$. For comparison, the dashed and dotted lines indicate the values of these quantities when surface tension is constant: $\sigma \equiv \sigma(0) = 72.8$ dyne cm^{-1} $(- - -)$ and $\sigma \equiv \sigma_E = 31$ dyne cm^{-1} $(\cdots)$.

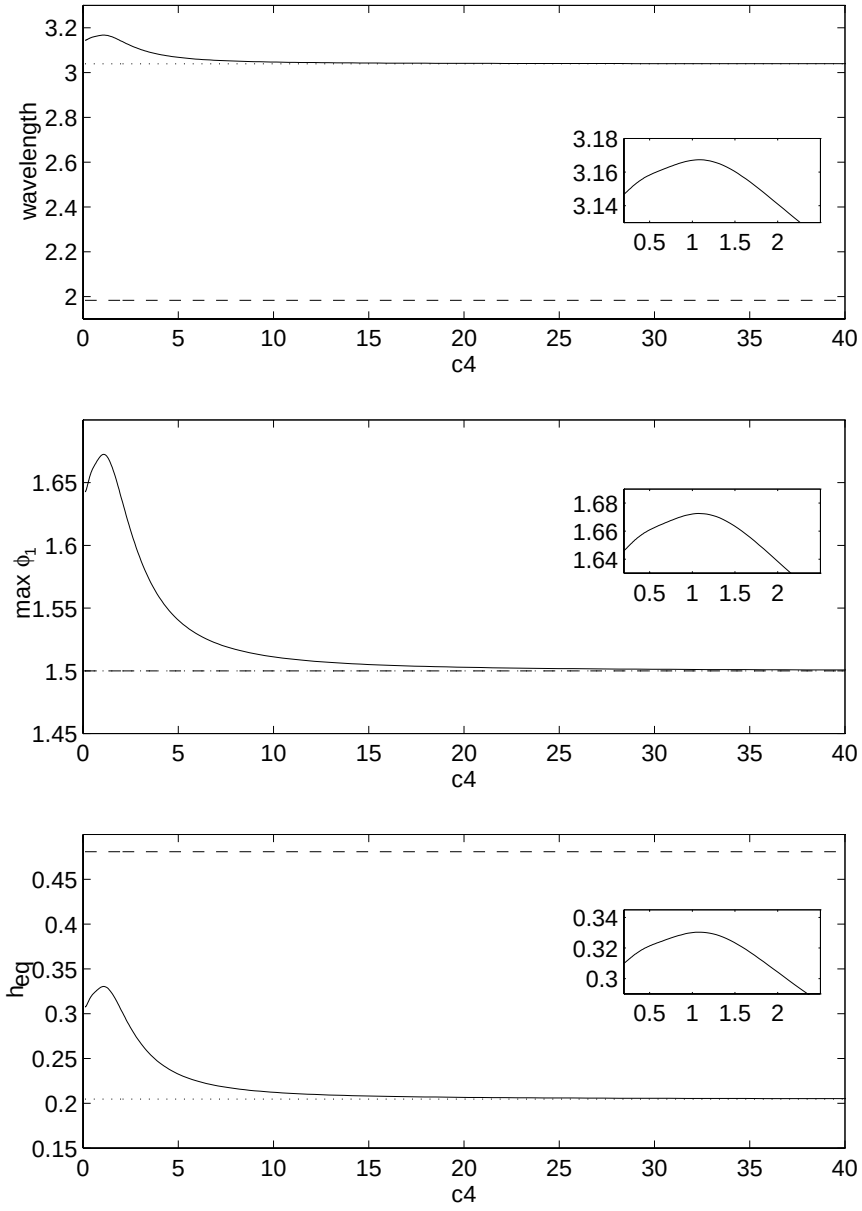

Figure 5: Dependence of the sustained farfield oscillation on c_4 of a jet with decaying surface tension given by the Brazee *et al.* form. The top, middle, and bottom graphs show the dependence of farfield wavelength, amplitude, and energy, respectively, for $c_4 > 0.1$. The dashed and dotted lines indicate the values of these quantities when surface tension is constant: $\sigma \equiv \sigma(0) = 72.8$ dyne cm^{-1} $(- - -)$ and $\sigma \equiv \sigma_E = 31$ dyne cm^{-1} $(\cdots)$.

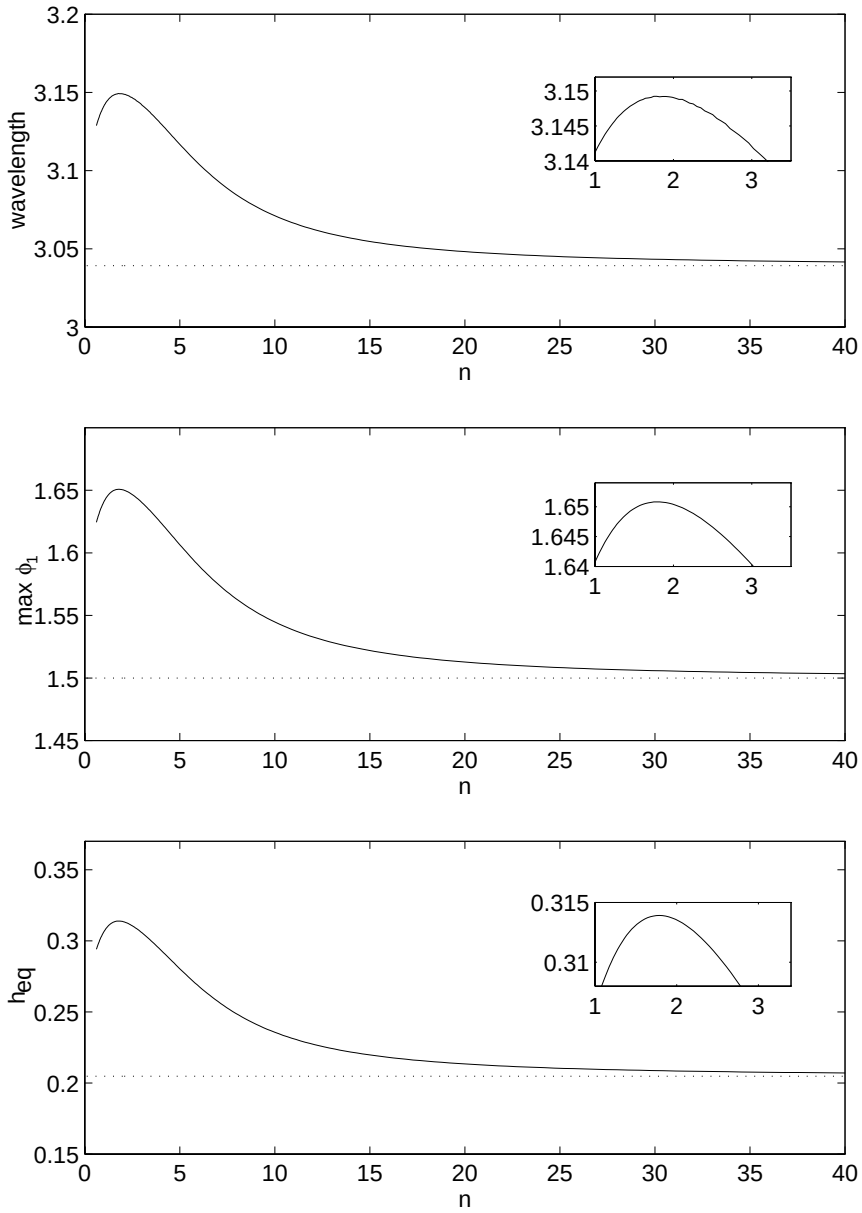

Figure 6: Dependence of the sustained farfield oscillation on n of a jet with decaying surface tension given by the Hua and Rosen form when $c_5 = 1.0$. The top, middle, and bottom graphs show the dependence of farfield wavelength, amplitude, and energy, respectively, for $n > 0.6$.

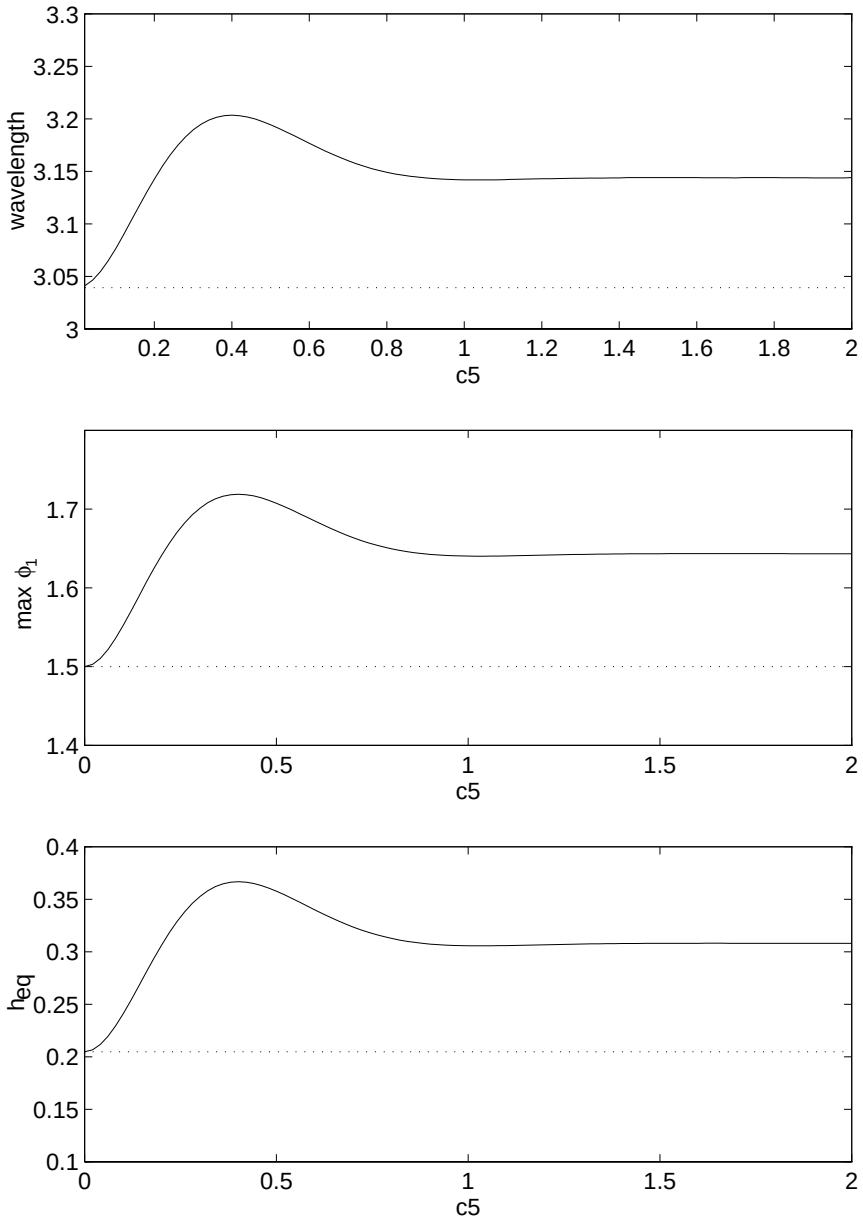

Figure 7: Dependence of the sustained farfield oscillation on c_5 of a jet with decaying surface tension given by the Hua and Rosen form when $n = 3.0$. The top, middle, and bottom graphs show the dependence of farfield wavelength, amplitude, and energy, respectively.

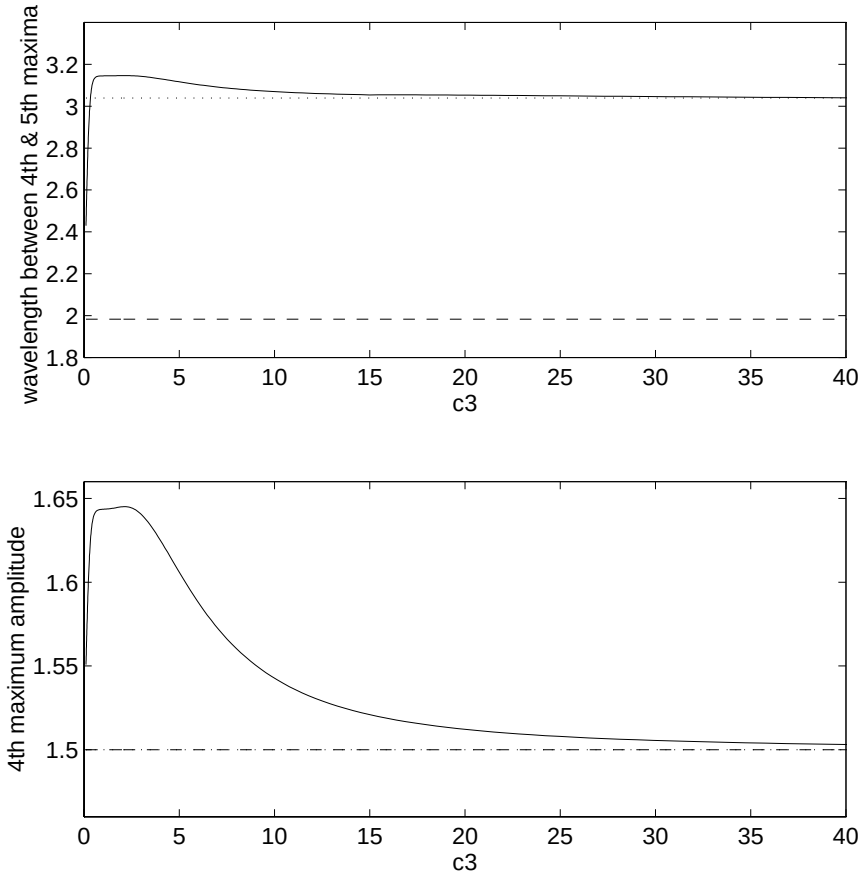

Figure 8: Dependence of the oscillation after four cycles on c_3 of a jet with exponentially decaying surface tension. The top graph shows the dependence of the wavelength between the fourth and fifth maxima on c_3; the bottom graph shows the dependence of the fourth maximum amplitude on c_3. For comparison, the dashed and dotted lines indicate the values of these quantities when surface tension is constant: $\sigma \equiv \sigma(0) = 72.8$ dyne cm^{-1} $(- - -)$ and $\sigma \equiv \sigma_E = 31$ dyne cm^{-1} $(\cdots)$.

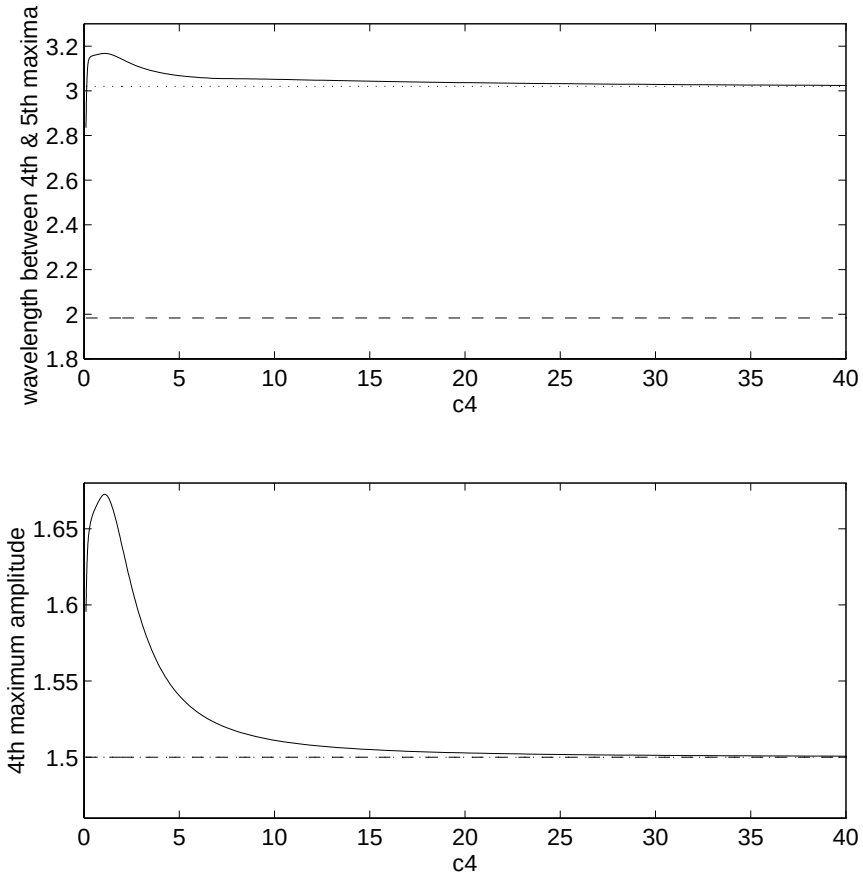

Figure 9: Dependence of the oscillation after four cycles on c_4 of a jet with decaying surface tension given by the Brazee *et al.* form. The top graph shows the dependence of the wavelength between the fourth and fifth maxima on c_4; the bottom graph shows the dependence of the fourth maximum amplitude for c_4.

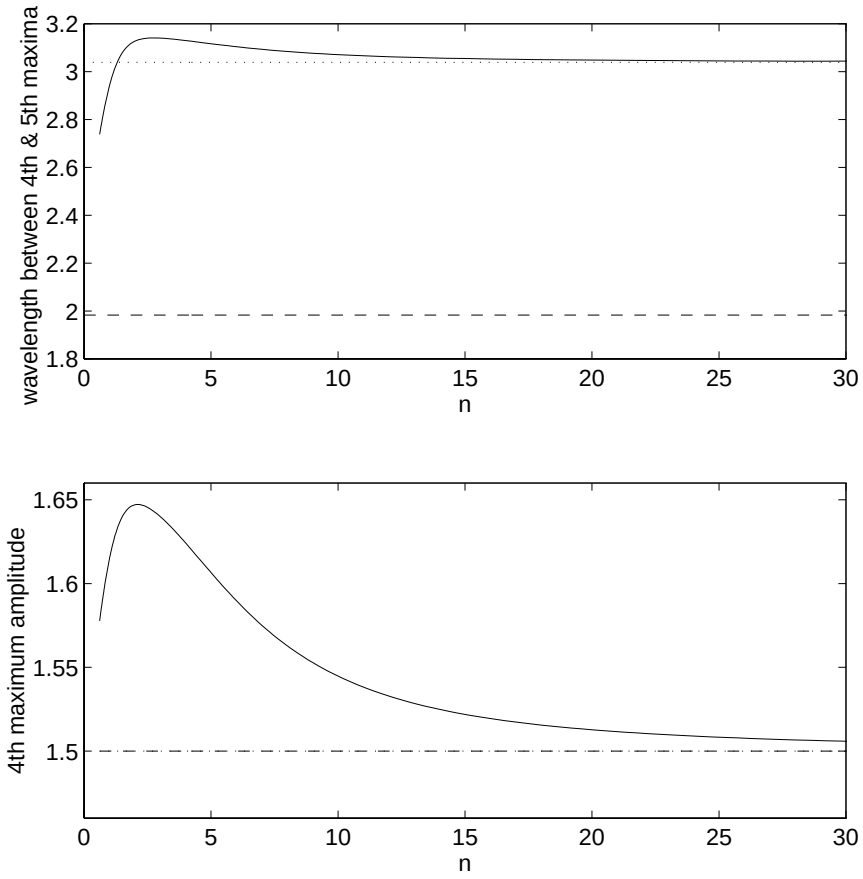

Figure 10: Dependence of the oscillation after four cycles on n of a jet with decaying surface tension given by the Hua and Rosen form. The top graph shows the dependence of the wavelength between the fourth and fifth maxima on n; the bottom graph shows the dependence of the fourth maximum amplitude on n.

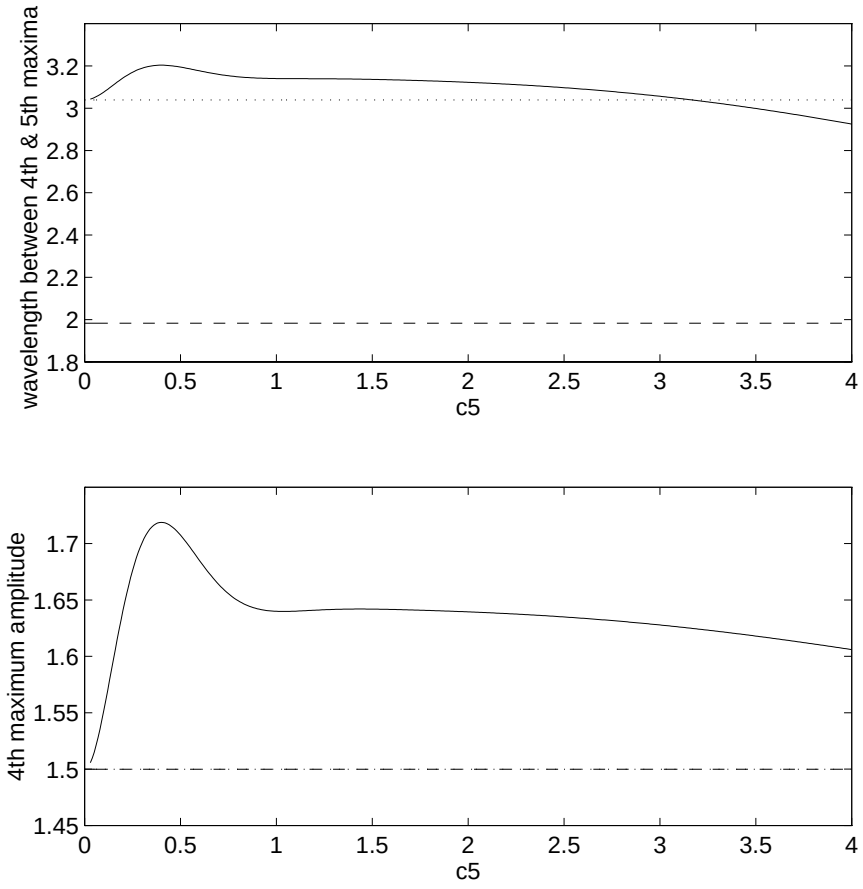

Figure 11: Dependence of the oscillation after four cycles on c_5 of a jet with decaying surface tension given by the Hua and Rosen form. The top graph shows the dependence of the wavelength between the fourth and fifth maxima on c_5; the bottom graph shows the dependence of the fourth maximum amplitude on c_5. These values are the farfield values for amplitude, and energy for $c_5 > 0.03$.

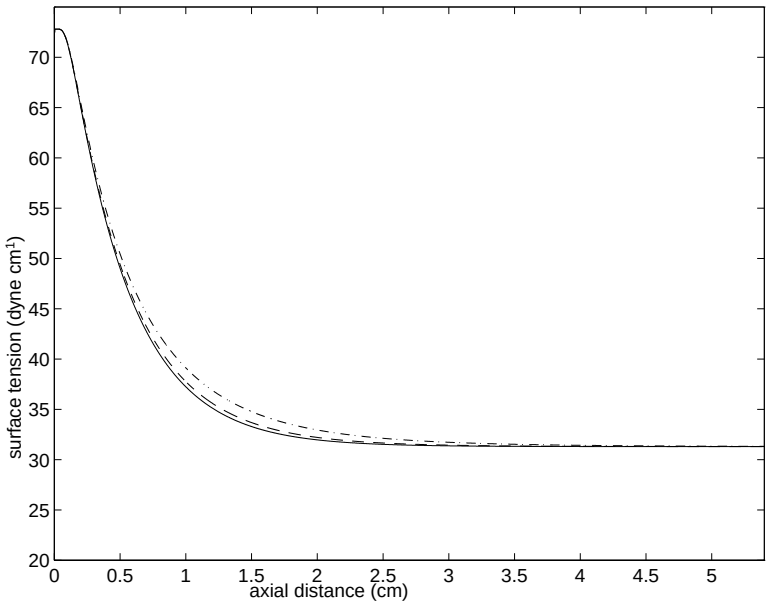

Figure 12: The effect of gravity on surface tension as a function of axial distance. Surface tension as a function of surface age is given by the Brazee *et al.* form with $c_4 = 2.75 \times 10^{-5}$: $F^{-1} = 0$ (——), $F^{-1} = 0.5$ (– – –), $F^{-1} = 2$ (_ .. _ .. _ .).

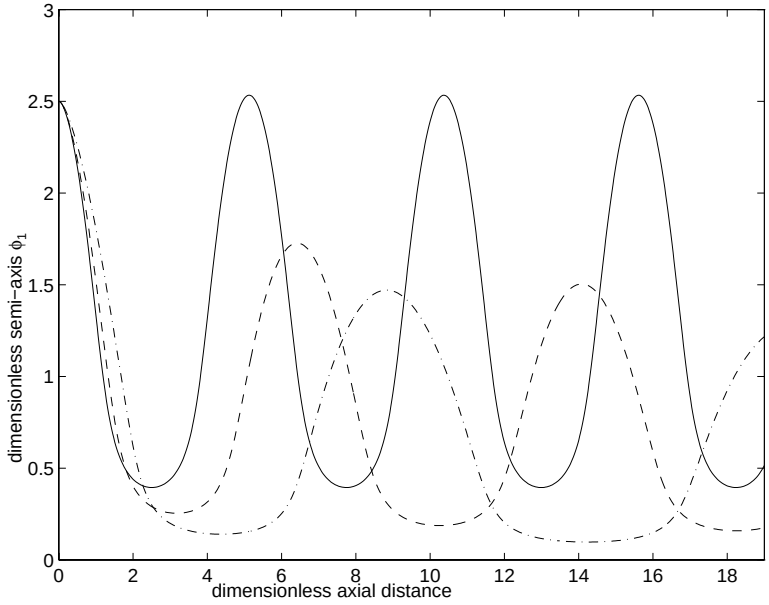

Figure 13: The effect of gravity on the oscillating jet profile with surface tension given by Figure 12. $\phi_1(0) = 2.5, \phi_{1,z}(0) = 0$, $R^{-1} = 0$, $F^{-1} = 0$ (——), $F^{-1} = 0.5$ (– – –), $F^{-1} = 2$ (_ . _ .).

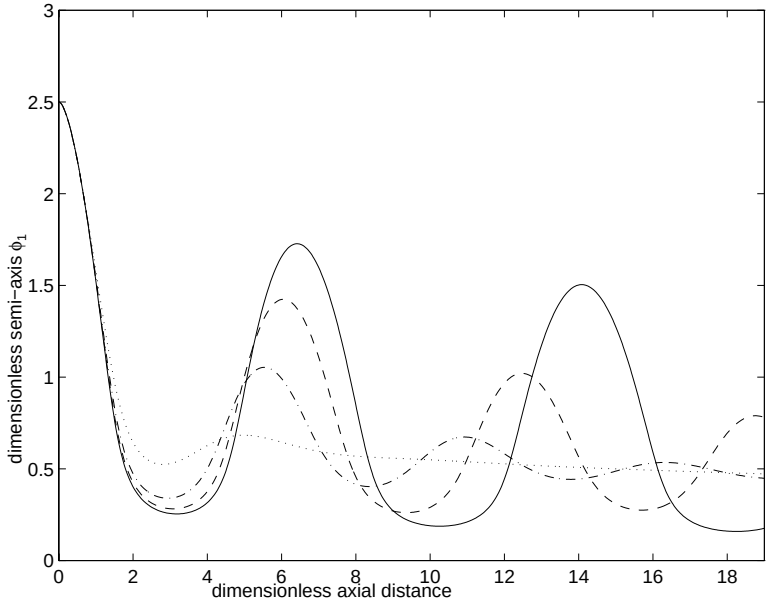

Figure 14: The effect of viscosity on the oscillating jet profile with surface tension given by Figure 12. $F^{-1} = 0.5$, $R^{-1} = 0$ (——), $R^{-1} = 0.0152$ (− − −), $R^{-1} = 0.045$ (_ _ _ _), $R^{-1} = 0.15$ ($\cdots$).